



# Evolution of functional groups and pore structure during cotton and corn stalks torrefaction and its correlation with hydrophobicity



Yingquan Chen<sup>a</sup>, Biao Liu<sup>a</sup>, Haiping Yang<sup>a,\*</sup>, Qing Yang<sup>b,\*</sup>, Hanping Chen<sup>a</sup>

<sup>a</sup> State Key Laboratory of Coal Combustion, Huazhong University of Science and Technology, Wuhan, Hubei 430074, PR China

<sup>b</sup> Department of New Energy Science and Engineering, Huazhong University of Science and Technology, Wuhan, Hubei 430074, PR China

## HIGHLIGHTS

- The broken of O–H bond and C–O bond in primary alcohol groups occurs preferentially.
- Until 230 °C, hydroxyl removal and generation of micropore are due to dehydration.
- Formation of carboxyl or conjugated ketone and reconstruction of pore occur followed.
- Hydrophobicity may have a highly linear correlation with hydroxyl and micropore.

## ARTICLE INFO

### Article history:

Received 11 April 2014

Received in revised form 8 July 2014

Accepted 15 July 2014

Available online 2 August 2014

### Keywords:

Torrefaction

Porosity

Hydroxyl group

Hydrophobicity

## ABSTRACT

The evolution of physicochemical structure of two stalks during torrefaction and its correlation with the hydrophobicity were investigated. Two-dimensional perturbation correlation infrared spectroscopy was used to study the evolution of functional groups. The pore structure of torrefied stalks was analyzed based on the isothermal adsorption of N<sub>2</sub> and CO<sub>2</sub>. During torrefaction, the removal of hydroxyl groups on the holocellulose resulted in dehydration and formation of carboxyl and conjugated ketone. The breaking of O–H bond and C–O bond in primary alcohol groups occurs preferentially for cotton stalk and corn stalk, respectively. Due to the modification of structure, the macropores diminished while more micropores formed. Equilibrium moisture content decreased significantly when torrefaction temperature increased, suggesting that hydrophobicity is improved by torrefaction. Meanwhile, the removal of hydroxyl and the formation of micropores had highly linear correlation with the formation of hydrophobicity. The result will be beneficial for better understanding of the mechanism of torrefaction and formation of hydrophobicity.

© 2014 Elsevier Ltd. All rights reserved.

## 1. Introduction

Biomass is an efficient, clean, and renewable energy source with near-zero emission of CO<sub>2</sub> and low pollutants emission [1]. However, the low bulk density, high moisture content, degradation during storage, and low energy density of biomass are critical challenges in using biomass as feedstock of combustion, gasification or pyrolysis [2,3]. Torrefaction, a thermal treatment carried out at the relatively low temperature ranging from 225 °C to 300 °C, may ameliorate these problems and enhance fuel properties of solid

biomass [4–6]. In the past several years, biomass torrefaction related to different types of biomass feedstock [7–12], operating condition [13–16], and the effect on the subsequent conversation [8,17–20], was intensively researched.

Meanwhile, to deeply understand the mechanism of torrefaction, the evolving structures during torrefaction have also been characterized. Based on FTIR and solid <sup>13</sup>C NMR analysis of torrefied corncobs, Zheng et al. [21] further confirmed that different transformation of the polymers would occur in agricultural straws similar to the torrefied wood [22] and the formation of cross-linking during cellulose torrefaction affected the bio-oil quality. Chang et al. [23] analyzed the torrefied sprucewood and bagasse using FTIR and XRD, and suggested that thermal decomposition of hemicellulose predominated over lignin decomposition and the cross-linking of cellulose in torrefaction. Several other FTIR analyses on different types of biomass [10,24–27] also confirmed that (1) hemicellulose is initially degraded by mild torrefaction at

\* Corresponding authors. Address: 1037 Luau Road, Wuhan, Hubei 430074, PR China. Tel.: +86 027 87542417x8211; fax: +86 027 87545526 (H. Yang). Tel./fax: +86 027 87558398 (Q. Yang).

E-mail addresses: [chyq721@qq.com](mailto:chyq721@qq.com) (Y. Chen), [liubiaoqc@foxmail.com](mailto:liubiaoqc@foxmail.com) (B. Liu), [yhpings2002@163.com](mailto:yhpings2002@163.com) (H. Yang), [qyang@hust.edu.cn](mailto:qyang@hust.edu.cn) (Q. Yang), [hp.chen@163.com](mailto:hp.chen@163.com) (H. Chen).

low temperature (<250 °C) while cellulose and lignin are degraded by severe torrefaction at high temperature (>250 °C) and (2) the increasing intensity of C—O—C band demonstrates that cross-linking reaction occurs during torrefaction.

However, conventional FTIR is mainly used to describe the interaction between the infrared beam and the sample, it is difficult to show the information on the significant peak overlaps, especially the fingerprint part, and it is difficult for the mechanistic assessments [28]. Recently, the generalized two-dimensional perturbation correlation infrared spectroscopy (2D-PCIS), put up by Noda, etc. was supposed to understand the evolution of chemical function groups of solid materials [29]. Harvey et al. [28] reported the application of 2D-PCIS on biochar formation process. It revealed that the primary reactions controlling biochar properties contain the defragmenting of lignocellulose H-bonding network and emethylenation/demethylation, oxidation, or dehydroxylation/dehydrogenation of lignocellulose fragments. In this study, the 2D-PCIS was introduced to the structure analysis of torrefied biomass, a deep understand of torrefaction mechanism would be obtained.

Not only the chemical structure changed during torrefaction for biomass, but also the physical structure, especially the pore structure, would be changed. However, in the previous works, the evolution of pore structure of torrefied biomass is rarely reported, which is not conducive to further understand the torrefaction mechanism. On the other hand, the changing of torrefied biomass during torrefaction is also reflected by the evolution of other properties such as the hydrophobic property. The hydrophobic property of torrefied biomass was determined by the chemical and physical structure [26,30–32].

Therefore, in this study, the 2D-PCIS was used to investigate the evolution of chemical structure of two agriculture straws during torrefaction, and the pore properties including the surface area, pore volume and pore size distribution, were analyzed. To understand deeply the formation mechanism of hydrophobic property, a quantitative correlation between these physicochemical structures and the hydrophobicity is calculated.

## 2. Materials and methods

### 2.1. Sample preparation and torrefaction

Cotton stalk and corn stalk were collected locally and naturally dried after being reaped. Straws samples were then stored in a storage room with good ventilation. The results of the fiber analysis and the ultimate analysis of raw, dry feedstock are presented in Table 1. The content of cellulose in cotton stalk is up to 53.57%, which is higher than that of corn stalk. On the other hand, corn stalk had higher content of hemicellulose (up to 40.44%), about twice of cotton stalk. The ultimate analysis shows that both these two stalks have high O content and low C content, although the contents of cellulose, hemicellulose and lignin of these two stalks are significantly different.

Torrefaction was carried out with a fixed bed comprising a vertical tube (I.D.: 38 mm and H: 600 mm), an electrical furnace, a gas condensing system, and an incondensable gas collection and analysis system. After the tube was pre-heated to selected

temperatures (200 °C, 230 °C, 260 °C and 290 °C), the sample (5 g, particle size: 2–3 cm) was quickly put into the center of the reactor and kept for 30 min. Pure N<sub>2</sub> (99.99%) was purged continuously to maintain an inert atmosphere and the flow rate was set at 1000 ml/min. The solid products were then cooled to ambient temperature. Each trial was repeated three times, and the subsequent analysis was based on the mixed products from these repeated experiments.

### 2.2. Characterization of physicochemical structure

#### 2.2.1. 2D-PCIS

The infrared spectrum of the samples between 4000 cm<sup>-1</sup> and 400 cm<sup>-1</sup> was recorded using a VERTEX 70 spectrometer (Bruker, Germany). Each spectrum was the result of 120 accumulated scans with 4 cm<sup>-1</sup> resolution, and the apodization function was the Happ-Genzel type. To prepare the pellet, approximately 0.7 mg of dried solid sample and 70 mg KBr (Merck, spectroscopy grade) were mixed, and the resulting mixture was pressed successively at pressures of 5 tons/cm<sup>2</sup> for 5 min and 10 tons/cm<sup>2</sup> for 5 min under vacuum.

Noda et al. [29] put forward the mathematical procedure and numerical computation of the 2D-PCIS spectroscopy in detail. A basic concept of 2D-PCIS spectroscopy is described below [28]. Firstly, consider a perturbation-induced change of the spectral intensity  $y(w, t)$  observed during an interval of external variable  $t$  between  $T_{\min}$  and  $T_{\max}$ , where  $w$  and  $T$  are wavenumber and perturbation of temperature, respectively. The change is expressed as follows:

$$\tilde{y}(w, t) = \begin{cases} y(w, t) - \bar{y}(w) & \text{for } T_{\min} \leq t \leq T_{\max} \\ 0 & \text{otherwise} \end{cases} \quad (1)$$

where  $\bar{y}(w)$  is the stationary or averaged spectrum defined by:

$$\bar{y}(w) = \frac{1}{T_{\max} - T_{\min}} \int_{T_{\min}}^{T_{\max}} y(w, t) dt \quad (2)$$

Secondly, the 2D correlation spectrum  $X(w_1, w_2)$  is expressed as:

$$X(w_1, w_2) = \langle \tilde{y}(w_1, t) \cdot \tilde{y}(w_2, t) \rangle \quad (3)$$

where  $X(w_1, w_2)$  represents the functional comparison of spectral intensity variations  $\tilde{y}(w, t)$  measured at different wavenumbers,  $w_1$  and  $w_2$ , during a fixed interval of the external temperature. The symbol  $\langle \rangle$  denotes the correlation function designed to compare the dependence of changes of spectral intensity,  $\tilde{y}(w, t)$ , at  $w_1$  and  $w_2$  on temperature Noda et al. [29] adopt a simple convention to treat  $X(w_1, w_2)$  as a complex number function:

$$X(w_1, w_2) = \Phi(w_1, w_2) + i\Psi(w_1, w_2) \quad (4)$$

where  $\Phi(w_1, w_2)$  and  $\Psi(w_1, w_2)$  denote synchronous and asynchronous 2D correlation intensity, respectively. The synchronous 2D correlation intensity  $\Phi(w_1, w_2)$  represents the overall similarity (in-phase or coincidental) between intensity changes in  $w_1$  and  $w_2$  when the external temperature  $T$  increases from  $T_{\min}$  to  $T_{\max}$ . On the other hand, the asynchronous 2D correlation intensity  $\Psi(w_1, w_2)$  is regarded as a measure of dissimilarity (out-of-phase or sequential) of the changes of spectral intensity in  $w_1$  and  $w_2$  on  $T$ .

**Table 1**  
The properties of the samples.

Sample	Chemical composition (d, wt.%)			Ultimate analysis (d, wt.%)					
	Hemicellulose	Cellulose	Lignin	Other	C	H	N	S	O
Cotton stalk	20.98	53.57	17.21	8.24	47.43	6.65	1.21	0.36	39.54
Cornstalk	40.44	34.6	7.79	17.17	44.94	6.54	1.28	0.34	38.22

Generally, the synchronous and asynchronous 2D correlation intensity are both represented as schematic contour maps where two types of peaks are represented as two different correlations. One is autopeak (on the  $w_1 = w_2$  diagonal), which is unique to the synchronous 2D correlation associated with positive correlation values and represents the vibrations most susceptible to changes in the external temperature  $T$ . The other is crosspeak (in off-diagonal positions,  $w_1 \neq w_2$ ) in the synchronous and asynchronous 2D spectrum associated with positive or negative correlation value and represent, respectively, the general direction and sequence of change in  $w_1$  compared to  $w_2$  with Harvey et al. [28] summarized the Noda's rules for interpreting cross peaks as shown in Table 1S in Supplementary Material. All of 2D-PCIS spectra were calculated by homemade software named "2Dshige" [28]. Here, a relative concentration ( $I_w/I_{max}$ ) for different functional groups in the raw and torrefied stalks was defined, where  $I_w$  was the IR intensity using Kubelka–Munk units at the characteristic wavenumber for a given functional group and  $I_{max}$  was the maximum intensity for the given functional groups across raw and torrefied samples from the same stalk.

### 2.2.2. Pore properties and $N_2/CO_2$ adsorption isotherms

$N_2$  adsorption at liquid nitrogen temperature (77 K) and  $CO_2$  adsorption at ice temperature (273 K) were carried out on a Micromeritics micropore analyzer (ASAP2020, USA). Before the adsorption measurements, the sample was degassed at 150 °C

under a vacuum (pressure of 50  $\mu$ m Hg) for 10 h. Based on the  $CO_2$ -adsorption isotherm, the micropore surface area was determined by the Dubinin–Astakhov equation derived from molecular fill theory. The pore-size distribution was analyzed by the density-function theory (DFT) method [33], which can be used to calculate the distribution of micro- (<2 nm), meso- (2–50 nm), and macropores (>50 nm) simultaneously. The DFT method is a molecular level statistical thermodynamic theory that relates the adsorption isotherm to the microscopic properties of the system: the fluid–fluid and fluid–solid interaction energy parameters, the pore size, the pore geometry, and the temperature [33]. Cumulative pore volume (CPV) is calculated by DFT.

### 2.3. Measurement of hydrophobicity

The equilibrium moisture content (EMC) was obtained using a controlled humidity chamber (Sengxin CORP, HWS-150, China) with relative humidity (RH) ranging from 50% to 90% at 30 °C. To obtain the EMC data at low RH (about 10% at 30 °C), the solid samples were exposed in the chamber where a saturated lithium chloride solution was used to maintain a constant humidity (about 10.9%). The solid samples (~2 g) were dried in a convection oven at 105 °C for 30 h, and then immediately transferred into these chambers, where the samples resided about 3–12 days to reach the equilibrium. After that, the samples were moved to an electrical oven at 105 °C, kept for 30 h and the EMC was determined.

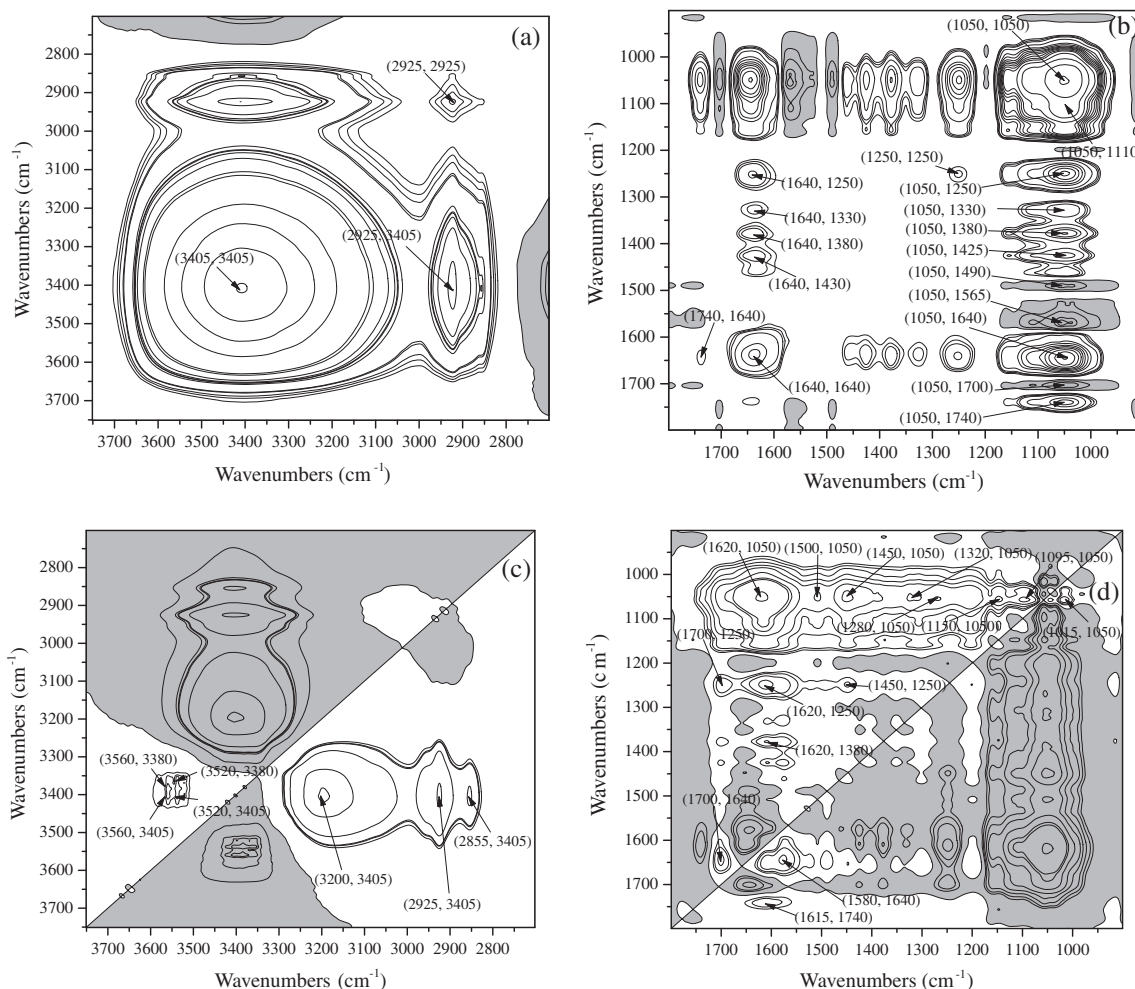


**Fig. 1.** 2D-PCIS spectra in the range of wavenumbers of 3750–2700  $cm^{-1}$  and 1800–900  $cm^{-1}$  analysis windows for torrefied cotton stalk (a and b) synchronous spectra and (c and d) asynchronous spectra. Light gray and white areas indicate negative and positive correlation values, respectively.

### 3. Results and discussions

#### 3.1. Evolution of functional group by 2D-PCIS FTIR

The FTIR spectra of torrefied stalks at different torrefaction temperature are shown in Fig. 1S. For both stalks, the intensity of hydroxyl around  $3500\text{--}3200\text{ cm}^{-1}$  is decreased when torrefaction severity increased; however, the intensity of hydrocarbon structure around  $3000\text{--}2800\text{ cm}^{-1}$  increased slightly, which might be due to the decomposition of hemicellulose. In the fingerprint region, the intensity of C–O stretch around  $1200\text{--}1000\text{ cm}^{-1}$  decreases but that of C=C and C=O stretches around  $1700\text{--}1500\text{ cm}^{-1}$  increase. The result is consistent with the previous works [21,25].

Figs. 1 and 2 show the 2D-PCIS spectra of cotton stalk and that of corn stalk, respectively. In the spectra, the line is a contour for the correlation value calculated by 2D-PCIS. If the contour has a high intensity, it means a correlation peak exists. Table 2 shows the oxygen-containing functional groups in raw and torrefied biomass identified by several previous studies [10,21,23–27]. At first, these functional groups susceptible to the increasing severity of torrefaction can be identified by the autopeaks in synchronous spectra. Based on the values of autopeaks, the different bonds show varied levels of change sensitivity. The top three susceptible bonds are H-bond in primary alcohol groups, C–O bond of primary alcohol group and C–O bond of second alcohol group, which are

similar to that of cotton stalk and corn stalk. This indicates that the change of hydroxyl in alcohol groups of sugar chain is the major reaction during torrefaction. However, the change of H-bond in primary alcohol groups is the most susceptible bond for cotton stalk, while the change of C–O bond of primary alcohol group is the most susceptible bond for corn stalk. It suggests that the path of bond breaking in hydroxyl is different. During torrefaction of cotton stalk, the O–H bonds in primary alcohol groups break preferentially because of the higher content of cellulose and lignin that is difficult to decompose. However, the C–O bonds in primary alcohol groups break preferentially in corn stalk due to the higher contents of hemicellulose. The change sensitivity of other bonds, such as C=C bond (in aromatic ring and unconjugated alkenes), C=O bond (in aldehyde, ketone and carboxyl), C–O bond (in ester and tertiary hydroxyl groups) and C–H bond (in methyl, methylene and aromatic ring), is lower than that of C–O bonds and O–H bonds in primary alcohol groups by about one or two orders of magnitude.

Secondly, based on the cross peaks of synchronous and asynchronous spectra, 2D-PCIS can provide the information about the correlation of the change direction of different groups. Figs. 3 and 4 show the variation in relative intensities of different groups for cotton stalk and corn stalk, respectively. The vibrations of these groups are determined by the cross peaks. As shown in Fig. 3, 4 types of changing trends (thereafter type I–IV) are observed in 13 vibrations. In the three vibrations that represent O–H bond and

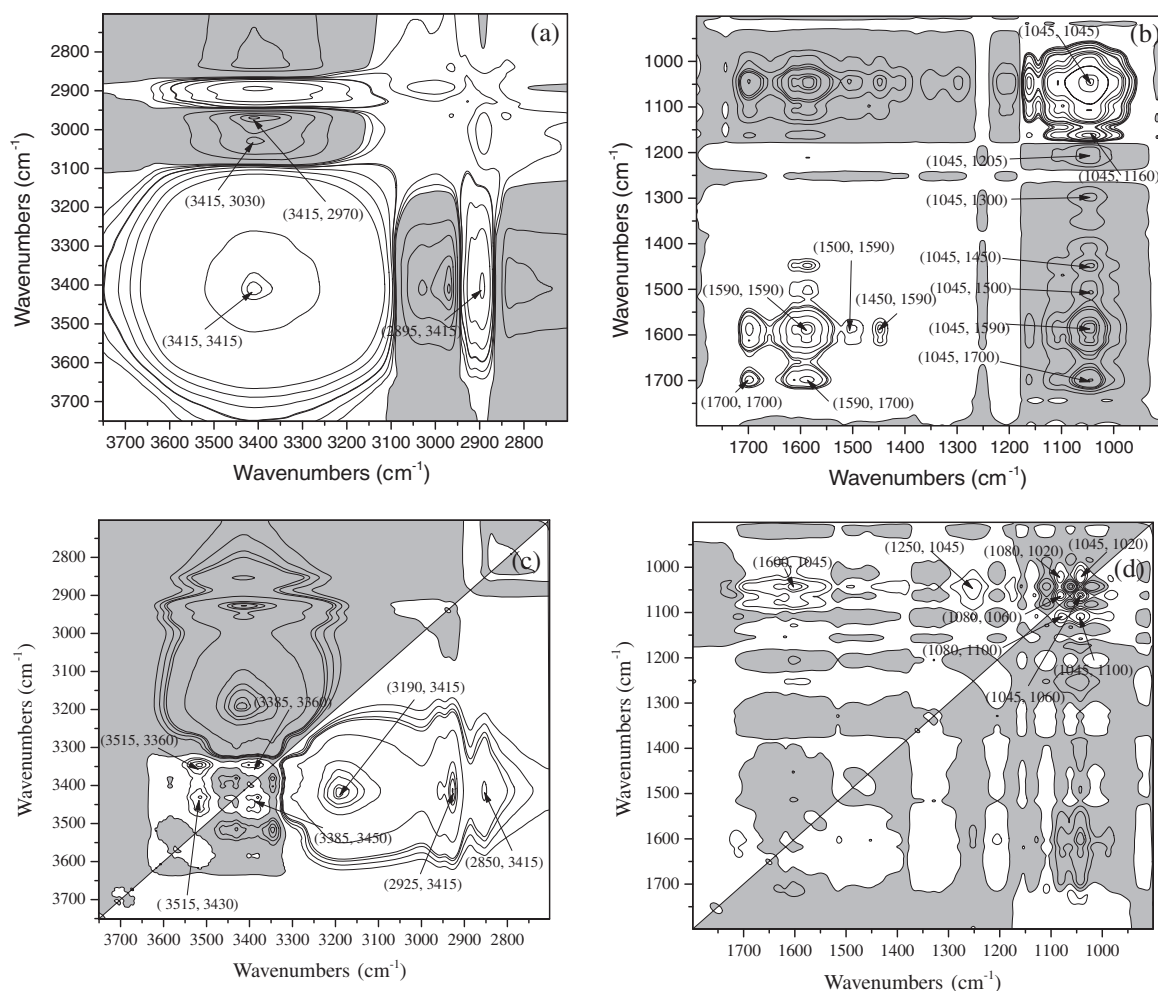
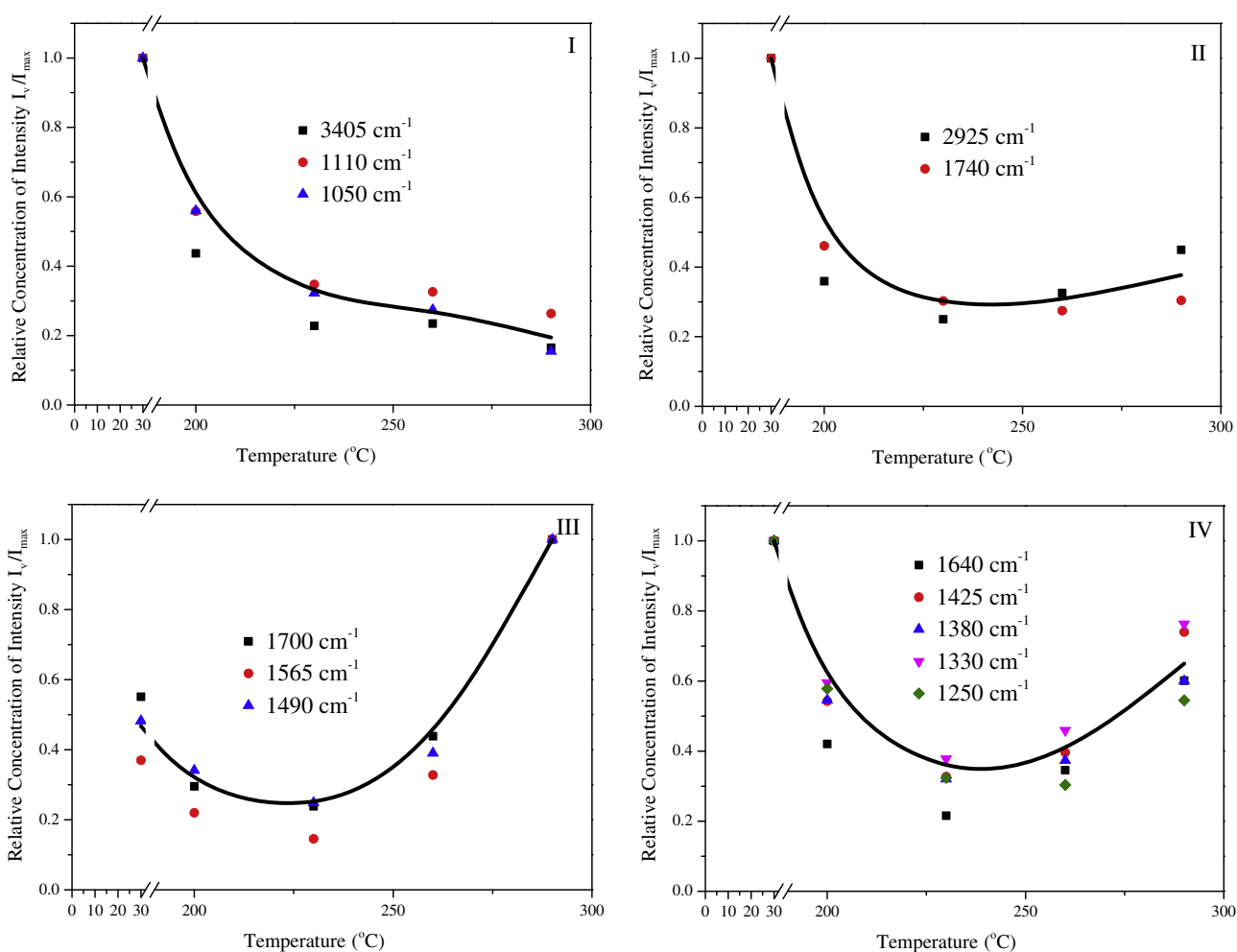


Fig. 2. 2D-PCIS spectra in the range of wavenumbers of  $3750\text{--}2700\text{ cm}^{-1}$  and  $1800\text{--}900\text{ cm}^{-1}$  analysis windows for torrefied corn stalk (a and b) synchronous spectra and (c and d) asynchronous spectra. Light gray and white areas indicate negative and positive correlation values, respectively.

**Table 2**  
The oxygen-containing functional groups in raw and torrefied biomass.

Wavenumbers ( $\text{cm}^{-1}$ )	Infrared absorption	Functional groups and structures
3415, 3405	O–H stretching	H-bonded formed by primary alcohol groups in cellulose or hemicellulose
3030	C–H stretching	Unconjugated alkenes
2970, 2925, 2895	C–H stretching	Aliphatic methylene
1740	C=O stretching	The carbonyl group in ketone
1700	C=O stretching	The carbonyl group in carboxyl or aldehyde
1640	C=C stretching	Linear unconjugated alkenes
1590	C=C stretching	Aromatic structures
1565, 1500	NH bending	Amides
1490, 1450, 1425	Aromatic C–C stretches	Aromatic structures
1380, 1330	C–H bending	Methyl, methylene
1300, 1250	C–O stretching	Benzoate esters
1205, 1160	C–O stretching	Tertiary hydroxyl group
1110	C–O stretching	Secondary hydroxyl group
1050, 1045	C–O stretching	Primary hydroxyl group



**Fig. 3.** Variation in relative intensities ( $I_v/I_{\max}$ ; for peaks in synchronous 2D-PCIS spectra) for raw and torrefied cotton stalk.

C–O bond in primary alcohol groups and C–O bond in secondary alcohol groups, the type I changing trend is observed, i.e. the relative intensity of vibrations decreases rapidly from 1 to 0.3 before 230 °C and decreases slightly from 0.3 to 0.2 after 230 °C with the increase of torrefaction severity. Since dehydration is considered as the major cause of the decrease of hydroxyl [34], it is reasonable to infer that dehydration may have finished before the torrefaction temperature reaches 230 °C. The relative intensity of vibrations in type II decreases rapidly from 1 to 0.3 until the

temperature reaches 230 °C but a subsequent slight increase from 0.3 to 0.4 is observed. Vibrations around 2925  $\text{cm}^{-1}$  and 1740  $\text{cm}^{-1}$  are characteristic of the C–H bond in methylene and C=O in carbonyl groups respectively and the intensities of these two vibrations decrease rapidly until 230 °C probably due to de-acetylation of hemicelluloses [22]. After the temperature reaches 230 °C, some new methylene and carbonyl groups could be generated resulting in the slight increase of the intensity of C–H and C=O bonds. The curve of type IV has a shape similar to that of type II although the

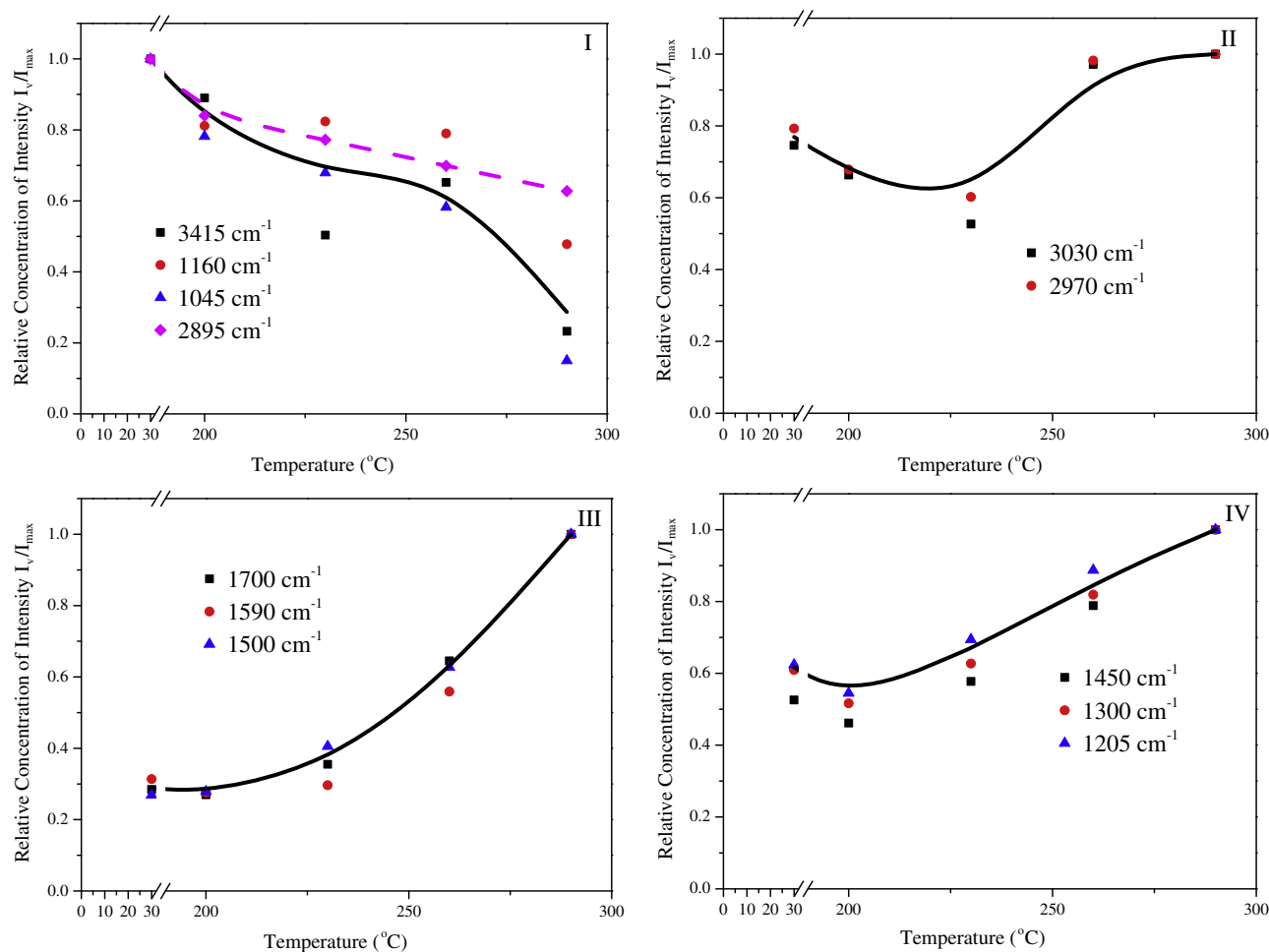


Fig. 4. Variation in relative intensities ( $I_v/I_{max}$ ; for peaks in synchronous 2D-PCIS spectra) for raw and torrefied corn stalk.

**Table 3**  
The specific surface area calculated from CO<sub>2</sub> adsorption ( $S_{DA}$ ) of raw and torrefied stalks (m<sup>2</sup>/g).

	Raw	200	230	260	290
Cotton stalk	73.6(2.1) <sup>a</sup>	80.4(1.6)	139.7(2.8)	101.7(2.1)	159.9(3.1)
Corn stalk	99.9(1.1)	106.5(1.3)	143.7(2.2)	136.0(3.7)	170.0(2.8)

<sup>a</sup> Number enclosed in the parenthesis were standard deviations with  $n = 3$ .

increasing section above 230 °C is steeper than that of type II. Furthermore, more vibrations belong to type IV, including C=O bond in conjugated ketone, aromatic C–C bond, C–H bond in methyl or methylene and C–O bond in benzoate esters. The intensities of these bonds, which may be part of lignin, have a decreasing trend until the temperature reaches 230 °C probably due to the slight cleavage of lignin branched chain. The intensity has an increasing trend above 230 °C probably due to the formation of new bonds from other structures. Different from the other three types, the curve of type III shows an increasing trend when torrefaction severity increases. Vibration around 1700 cm<sup>-1</sup> is characteristic of the C=O bond in aldehyde or carboxyl, and the increase of its relative intensity during torrefaction may be due to the oxidation of primary alcohol in cellulose and hemicellulose [28]. Vibrations around 1565 cm<sup>-1</sup> and 1490 cm<sup>-1</sup> are characteristic of the N–H bond in amides and aromatic C–C bonds. The increase of relative intensity of these two bonds may be due to concentrated effect when a large amount of hydroxyl is removed.

As shown in Fig. 4, except type III, the changing trends of the other three types of corn stalk are distinct from that of cotton stalk. At first, until 230 °C, the bond intensity in type I, II and IV decrease slightly, which suggests that the decomposition of corn stalk is relatively mild. However, when torrefaction temperature increases from 230 °C to 260 °C, it is observed that the bond intensities decrease sharply in the curve of type I but increase in the curve of type II and IV. Similar to cotton stalk, the changing trends of O–H bond and C–O bond in primary alcohol groups and C–O bond in secondary alcohol groups are of type I. According to the asynchronous spectra, the changes of these three bonds most likely occur before the changes of other bonds. It suggests that some other groups may be formed from the transformation of hydroxyl in the alcohol groups on the sugar chain during torrefaction for corn stalk, different with the dehydration of cotton stalk. Secondly, the vibrations in these types are different. Vibration around 3030 cm<sup>-1</sup>, which represents the C–H bond in unconjugated alkenes, is observed and replaced by vibration around 1740 cm<sup>-1</sup> in type II. Vibration around 1590 cm<sup>-1</sup>, which represents the new formed C=C bond in aromatic ring, is observed in type III. Three vibrations are not observed in type IV. It suggests that the path of change of three component of fiber in corn stalk is different with that of cotton stalk.

Harvey et al. used the 2D-PCIS on the biochar formation process under oxygen-limited conditions along a heat-treatment-temperature gradient (HTT; 200–650 °C) [28]. In our work, the heat-treatment-temperature gradient is 200–290 °C, which is different from Harvey et al.'s work. Under different treatment conditions,

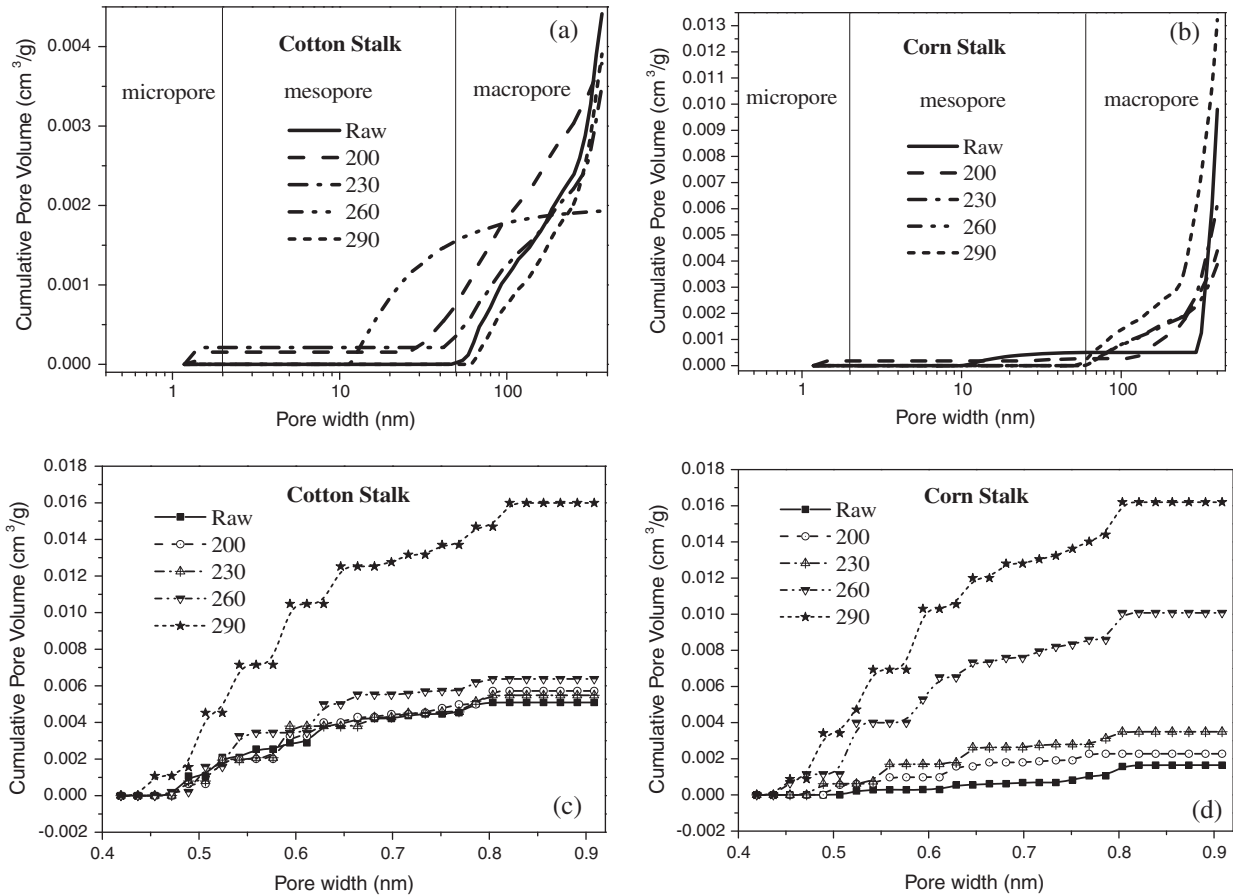


Fig. 5. Pore size distribution by DFT method based on N<sub>2</sub> and CO<sub>2</sub> isotherm adsorption for torrefied cotton stalk and corn stalk, (a and b) are calculated from N<sub>2</sub> adsorption while (c and d) are calculated from CO<sub>2</sub> adsorption for cotton stalk and corn stalk, respectively.

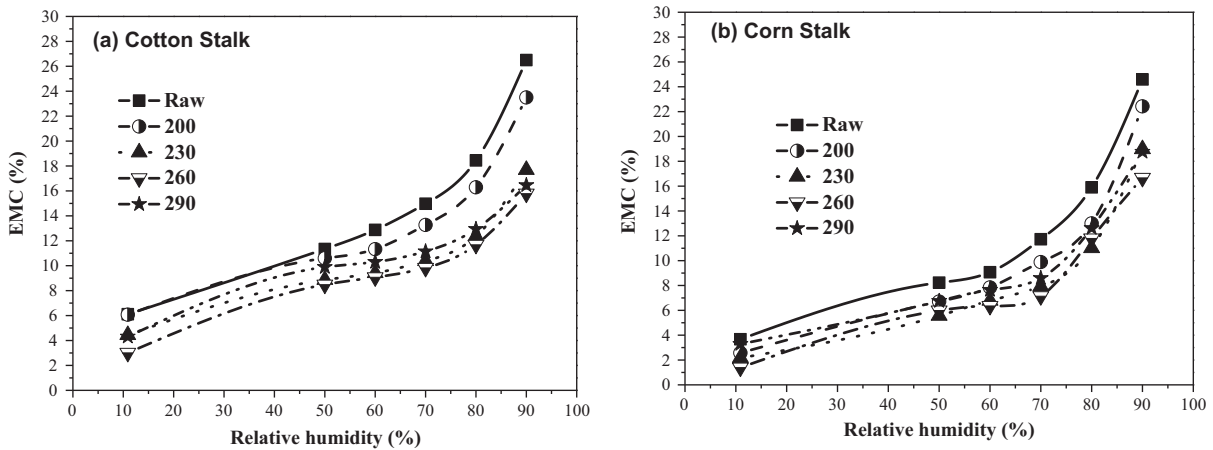


Fig. 6. The EMC of raw and torrefied stalks (a) cotton stalk and (b) corn stalk.

the similarity or dissimilarity between changes in the intensity at vibrations ( $\nu_1$  and  $\nu_2$ ) would be different. In addition, the range of vibration investigated in Harvey et al.'s work was 3700–2700  $\text{cm}^{-1}$ , and but our work focuses on the range from 3700  $\text{cm}^{-1}$  to 900  $\text{cm}^{-1}$ . However, our finding that the dehydration of hydroxyl of hemicellulose or cellulose may form carboxyl is consistent with Harvey et al.'s work.

### 3.2. Evolution properties of pore structure

The specific surface area of the raw and torrefied stalks are shown in Table 3. Probably because at the higher adsorption

temperature of CO<sub>2</sub>, the CO<sub>2</sub> molecule can more easily enter the micropores [33]. The changing trends of  $S_{DA}$  that until 230 °C some new pores may be generated during the dehydration according to the analysis in Section 3.1 but the damage of polymer structure of biomass constituent [22,27] may reduce the amount of pores at 260 °C. New pores would be formed when torrefaction severity increases.

The pore size distribution (PSD) based on N<sub>2</sub> adsorption and DFT analysis of torrefied biomass are shown in Fig. 5(a and b). The classification of micro-, meso-, and macropores follow the standards of International Union of Pure and Applied Chemistry, which stipulate that micropores are smaller than 2 nm, macropores are larger

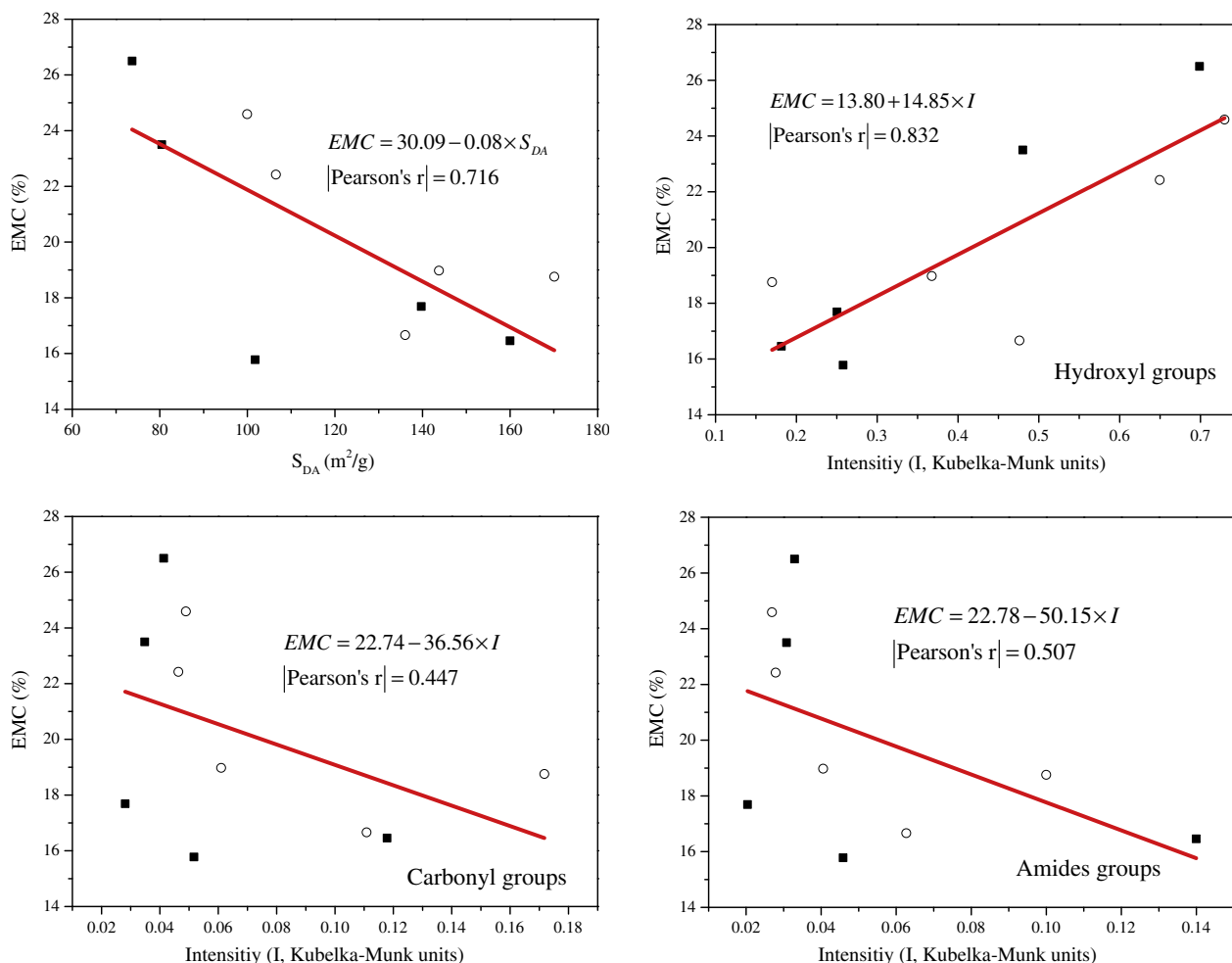


Fig. 7. The significant correlation of EMC and physicochemical structure of raw and torrefied stalks. ■ cotton stalk; ○ corn stalk.

than 50 nm, and the mesopores range from 2 to 50 nm. The micropores and mesopores are not observed in raw stalks. The macropores from 100 nm to 330 nm are the major pores for raw cotton stalk and the macropores above 300 nm are the major pores for raw corn stalks; these macropores may form during the lifetime of the biomass. It is observed that the number of original macropores of torrefied biomass at 200 °C decreases while mesopores (3–8 nm) appear. The amount of volatile released is negligible at 200 °C; therefore, the pores disappear probably due to the restructuring of the polymer, especially the hemicelluloses. However, the presence of mesopores needs further investigation. Up to 230 °C, an obvious degradation of hemicelluloses occurs, then significant number of new pores are formed in cotton stalk but few pores are formed in corn stalk. The degree of degradation of hemicellulose is further increased until 260 °C, and significant gaseous volatiles are observed during the experiment. However, the macropores rapidly disappear, and many mesopores (10–50 nm) are generated. It suggests that the polymer of three-component is damaged during degradation of hemicellulose and some large fragment may block the original macropores of raw biomass. With the further increase of temperature, the large fragment blocking the macropores might be released; as a result, in torrefied biomass at 290 °C, a large number of macropores are formed. Because of the liquid nitrogen temperature, the molecule momentum of N<sub>2</sub> is not sufficient to penetrate the little micropores of raw and torrefied biomass. The results of PSD analysis based on CO<sub>2</sub> adsorption and DFT method are shown in Fig. 5(c and d). With the increase of torrefaction temperature, the number of micropores increases,

and the center of pores in PSD shifts to smaller sizes (0.4 and 0.5 nm). The shift suggests that the degree of depolymerization increases with the increase of torrefaction temperature.

### 3.3. The evolution of hydrophobicity

The EMC measurement conducted in the controlled humidity chamber was duplicated, to test for reproducibility. The EMC value was reproducible within ±1.5%. Small growth of fungi on several samples at the completion of the EMC experiment were also observed [35], which could affect the structure of the stalk and influence the accuracy of the EMC data. But, this is inevitable because the environment of EMC experiment is suitable for the fungi growth and the hemicellulose in these samples is not completely degraded. Fig. 6 shows the dependence of EMC data on RH of raw torrefied stalks. At first, the EMC of torrefied stalks decreases with the increase of torrefaction temperature from 200 °C to 260 °C. The EMC increases slightly at 290 °C. Some previous reports suggested that the EMC performance of torrefied samples may be affected by the chemical and physical properties [26,30,35,36]. However, these works did not provide detailed information about how these properties influence the EMC. To understand the influence of the chemical and physical structure, the correlation between EMC and chemical-physical properties was calculated.

Figs. 7 and 2S show the significant and weak correlation between EMC and chemical-physical properties of raw and torrefied stalks, respectively. Based on the Pearson correlation

coefficients (Pearson's  $r$ ) between EMC and physical–chemical structure, the amount of micropore ( $S_{DA}$ ) and the intensity of hydroxyl group had a highly linear correlation with EMC. The negative correlation between  $S_{DA}$  and EMC suggests that the micropores formed during torrefaction may increase the hydrophobicity of torrefied stalks, while the positive correlation shows that the decrease of hydroxyl group may cause the decrease of EMC for torrefied stalks, which is consistent with the previous reports [26,30,36].

Therefore, the EMC of torrefied stalks decreases with the increase of torrefaction temperature from 200 °C to 260 °C probably due to the decrease of hydroxyl contents and the increasing amount of hydrophobic micropores. However, the formation of carbonyl in carboxyl and the new mesopore or macropores may have contributed to the slight increase of EMC at 290 °C.

#### 4. Conclusion

In this study, 2D-PCIS was used to analyze the FTIR spectra from raw and torrefied stalks. The removal of hydroxyl is the major reaction during torrefaction. Until the temperature reaches 230 °C, dehydration contributes to the removal of hydroxyl and generation of micropores. Subsequently, hydroxyl is transformed to carboxyl and conjugated ketone and pore structure is reconstructed. With the increase of the severity of torrefaction, the EMC decreases. The correlation between EMC and physicochemical structure shows that improved hydrophobicity may not only result by the removal of hydroxyl but also be caused by the formation of micropores and diminish of macropores.

#### Acknowledgements

The authors wish to express the great appreciation of the financial support from Key Projects of National Fundamental Research Planning (2013CB228102), Special Fund for Agro-scientific Research in the Public Interest (201303095) and National Natural Science Foundation of China (51376076, 51306067). We are also grateful for the technical support from Analytical and Testing Center in Huazhong University of Science & Technology (<http://atc.hust.edu.cn>). Mr. Ho Simon Wang has helped improve the linguistic presentation of the manuscript.

#### Appendix A. Supplementary material

Supplementary data associated with this article can be found, in the online version, at <http://dx.doi.org/10.1016/j.fuel.2014.07.036>.

#### References

- [1] Chen Y, Yang H, Wang X, Zhang S, Chen H. Biomass-based pyrolytic polygeneration system on cotton stalk pyrolysis: influence of temperature. *Bioresour Technol* 2012;107:411–8.
- [2] Uslu A, Faaiz APC, Bergman PCA. Bergman, pre-treatment technologies, and their effect on international bioenergy supply chain logistics. *Techno-economic evaluation of torrefaction, fast pyrolysis and pelletisation*. *Energy* 2008;33:1206–23.
- [3] Kargbo FR, Xing JJ, Zhang YL. Pretreatment for energy use of rice straw: a review. *Afr J Agric Res* 2009;4:1560–5.
- [4] Bridgeman TG, Jones JM, Shield I, Williams PT. Torrefaction of reed canary grass, wheat straw and willow to enhance solid fuel qualities and combustion properties. *Fuel* 2008;87:844–56.
- [5] Kiel JHA, Verhoeff F, Gerhauser H, Meuleman B. Vdi, torrefaction-based BO(2)-technology for biomass upgrading into commodity solid fuel pilot-scale testing and demonstration. In: *Strom Und Warme Aus Biogenen Festbrennstoffen*, V D I-V D E – Verlag GmbH, Dusseldorf, 2008. p. 43–51.
- [6] Deng J, Wang GJ, Kuang JH, Zhang YL, Luo YH. Pretreatment of agricultural residues for co-gasification via torrefaction. *J Anal Appl Pyrolysis* 2009;86:331–7.
- [7] Ben HX, Ragauskas AJ. Torrefaction of loblolly pine. *Green Chem* 2012;14:72–6.
- [8] Chen WH, Du SW, Tsai CH, Wang ZY. Torrefied biomasses in a drop tube furnace to evaluate their utility in blast furnaces. *Bioresour Technol* 2012;111:433–8.
- [9] Larsson SH, Rudolfsson M, Nordwaeger M, Olofsson I, Samuelsson R. Effects of moisture content, torrefaction temperature, and die temperature in pilot scale pelletizing of torrefied Norway spruce. *Appl Energy* 2013;102:827–32.
- [10] Shang L, Ahrenfeldt J, Holm JK, Sanadi AR, Barsberg S, Thomsen T, et al. Changes of chemical and mechanical behavior of torrefied wheat straw. *Biomass Bioenergy* 2012;40:63–70.
- [11] Shang L, Nielsen NPK, Dahl J, Stelte W, Ahrenfeldt J, Holm JK, et al. Quality effects caused by torrefaction of pellets made from Scots pine. *Fuel Process Technol* 2012;101:23–8.
- [12] Uemura Y, Omar WN, Tsutsui T, Yusup SB. Torrefaction of oil palm wastes. *Fuel* 2011;90:2585–91.
- [13] Bates RB, Ghoniem AF. Biomass torrefaction: modeling of volatile and solid product evolution kinetics. *Bioresour Technol* 2012;124:460–9.
- [14] Chen WH, Ye SC, Sheen HK. Hydrothermal carbonization of sugarcane bagasse via wet torrefaction in association with microwave heating. *Bioresour Technol* 2012;118:195–203.
- [15] Dhungana A, Basu P, Dutta A. Effects of reactor design on the torrefaction of biomass. *J Energy Resour Technol-Trans ASME* 2012;134:1–11.
- [16] Wang CW, Peng JH, Li H, Bi XTT, Legros R, Lim CJ, et al. Oxidative torrefaction of biomass residues and densification of torrefied sawdust to pellets. *Bioresour Technol* 2013;127:318–25.
- [17] Chen WH, Cheng WY, Lu KM, Huang YP. An evaluation on improvement of pulverized biomass property for solid fuel through torrefaction. *Appl Energy* 2011;88:3636–44.
- [18] Fisher EM, Dupont C, Darvell LI, Commandre JM, Saddawi A, Jones JM, et al. Combustion and gasification characteristics of chars from raw and torrefied biomass. *Bioresour Technol* 2012;119:157–65.
- [19] Rousset P, Aguiar C, Labbe N, Commandre JM. Enhancing the combustible properties of bamboo by torrefaction. *Bioresour Technol* 2011;102:8225–31.
- [20] Wannapeera J, Fungtammasan B, Worasuwannarak N. Effects of temperature and holding time during torrefaction on the pyrolysis behaviors of woody biomass. *J Anal Appl Pyrolysis* 2011;92:99–105.
- [21] Zheng AQ, Zhao ZL, Chang S, Huang Z, Wang XB, He F, et al. Effect of torrefaction on structure and fast pyrolysis behavior of corncobs. *Bioresour Technol* 2013;128:370–7.
- [22] Melkior T, Jacob S, Gerbaud G, Hediger S, Le Pape L, Bonnefois L, et al. NMR analysis of the transformation of wood constituents by torrefaction. *Fuel* 2012;92:271–80.
- [23] Chang S, Zhao ZL, Zheng AQ, He F, Huang Z, Li HB. Characterization of products from torrefaction of sprucewood and bagasse in an auger reactor. *Energy Fuels* 2012;26:7009–17.
- [24] Via BK, Adhikari S, Taylor S. Modeling for proximate analysis and heating value of torrefied biomass with vibration spectroscopy. *Bioresour Technol* 2013;133:1–8.
- [25] Zheng AQ, Zhao ZL, Chang S, Huang Z, He F, Li HB. Effect of torrefaction temperature on product distribution from two-staged pyrolysis of biomass. *Energy Fuels* 2012;26:2968–74.
- [26] Tapasvi D, Khalil R, Skreiberg O, Tran KQ, Gronli M. Torrefaction of Norwegian birch and spruce: an experimental study using macro-TGA. *Energy Fuels* 2012;26:5232–40.
- [27] Chen WH, Lu KM, Tsai CM. An experimental analysis on property and structure variations of agricultural wastes undergoing torrefaction. *Appl Energy* 2012;100:318–25.
- [28] Harvey OR, Herbert BE, Kuo L-J, Louchouart P. Generalized two-dimensional perturbation infrared spectroscopy reveals mechanisms for the development of surface charge and recalcitrance in plant-derived biochars. *Environ Sci Technol* 2012;46:10641–50.
- [29] Noda I, Dowrey AE, Marcott C, Story GM, Ozaki Y. Generalized two-dimensional correlation spectroscopy. *Appl Spectrosc* 2000;54:236A–48A.
- [30] Li H, Liu XH, Legros R, Bi XTT, Lim CJ, Sokhansanj S. Torrefaction of sawdust in a fluidized bed reactor. *Bioresour Technol* 2012;103:453–8.
- [31] Sarvaramini A, Gravel O, Larachi F. Torrefaction of ionic-liquid impregnated lignocellulosic biomass and its comparison to dry torrefaction. *Fuel* 2013;103:814–26.
- [32] Li H, Liu XH, Legros R, Bi XTT, Lim CJ, Sokhansanj S. Pelletization of torrefied sawdust and properties of torrefied pellets. *Appl Energy* 2012;93:680–5.
- [33] Feng B, Bhatia SK. Variation of the pore structure of coal chars during gasification. *Carbon* 2003;41:507–23.
- [34] Boateng AA, Mullen CA. Fast pyrolysis of biomass thermally pretreated by torrefaction. *J Anal Appl Pyrolysis* 2013;100:95–102.
- [35] Acharjee TC, Coronella CJ, Vasquez VR. Effect of thermal pretreatment on equilibrium moisture content of lignocellulosic biomass. *Bioresour Technol* 2011;102:4849–54.
- [36] Hakkou M, Petrisans M, Gerardin P, Zoulalian A. Investigations of the reasons for fungal durability of heat-treated beech wood. *Polym Degrad Stabil* 2006;91:393–7.